PCCP

Cite this: *Phys. Chem. Chem. Phys.*, 2011, **13**, 13656–13669

www.rsc.org/pccp

PAPER

Quantum stereodynamics of Li + HF reactive collisions: the role of reactants polarization on the differential cross section†

L. González-Sánchez,[a] O. Vasyutinskii,[b] A. Zanchet,[c] C. Sanz-Sanz[c] and O. Roncero*[c]

Received 8th November 2010, Accepted 9th May 2011
DOI: 10.1039/c0cp02452j

A complete quantum study for the state-to-state Li + HF(v,j,m) → LiF(v',j',Ω') + H reactive collisions has been performed using a wave packet method, for different initial rotational states and helicity states of the reactants. The state-to-state differential cross section has been simulated, and the polarization of products extracted. It is found that the reactivity is enhanced for nearly collinear collisions, which produces a vibrational excitation of HF, needed to overcome the late barrier. It is also found that LiF(v' = 0) products are preferentially forward scattered, while vibrationally excited LiF(v' = 1 and 2) are backward scattered. These results are interpreted with a simple reaction mechanism, based on the late character and bent geometry of the transition state, originating from a covalent/ionic crossing, which consists of two steps: the arrival at the transition state and the dissociation. In the first step, in order to get to the saddle point some HF vibrational excitation is required, which favors head-on collisions and therefore low values of m. In the second step a fast dissociation of H atom takes place, which is explained by the ionic Li^+F^-H character of the bent transition state: the FH^- is repulsive making that H depart rapidly leaving a highly rotating LiF molecule. For the higher energy analyzed, where resonances slightly contribute, the orientation and alignment of product rotational states, referred to as reactants frame (with the z-axis parallel to **k**), are approximately constant with the scattering angle. The alignment is close to −1, showing that **j**′ is perpendicular to **k**, while starting from initial states with well defined rotational orientation, as states with pure m values, the final rotational are also oriented. It is also found that when using products frame (with the z'-axis parallel to **k**′) the rotational alignment and orientation of products varies a lot with the scattering angle just because the z' axis changes from being parallel to anti-parallel to **k** when varying from θ = 0 to π.

I. Introduction

The anisotropic character of intermolecular interactions makes the orientation between reactants key for producing a reactive collision. Theoretically this orientation can be analysed studying the correlation of the four principal vectors; the two velocity vectors between reactants and products, **k** and **k**′, and the two angular momenta associated as well to reactants and products, **j** and **j**′. The correlation between the velocity vectors, **k**–**k**′, is directly related to the differential cross section (DCS) measured in crossed beam experiments, which has made these kinds of studies of high interest.[1–5]

Experimentally there are several techniques, such as deflection in homogeneous electric fields,[6] Doppler profile laser induced fluorescence[7] and resonance enhanced multiphoton ionization time-of-flight which, in addition to the angular resolution, can measure the final rotational polarization of products, involving the analysis of the correlation of three vectors **k**–**k**′–**j**′. From a theoretical point of view, the analysis of the three vector correlation **k**–**k**′–**j**′ may clarify the dynamics but complicates the simulations, since detailed state-to-state calculations should be required.

The production and control of the reactant rotational orientation is rather complicated experimentally, but it provides very valuable information about the entrance channel as well as a way to control the outcome of reactions.[8] The experimental techniques mainly used to produce the orientation of reactants make use of hexapole inhomogeneous electric fields;[9,10] absorption of linearly polarized radiation;[11,12] or the

[a] *Departamento de Química Física, Facultad de Ciencias Químicas, Universidad de Salamanca, 37008 Salamanca, Spain*
[b] *Ioffe Physico-Technical Institute, Russian Academy of Sciences, 194021 St. Petersburg, Russia*
[c] *Instituto de Física Fundamental, C.S.I.C., Serrano 123, 28006 Madrid, Spain. E-mail: oroncero@iff.csic.es*

† This article was submitted as part of a Themed Issue on molecular collision dynamics. Other papers on this topic can be found in issue 18 of vol. 13 (2011). This issue can be found from the *PCCP* homepage [http://www.rsc.org/pccp].

ones using the brute force with strong electric fields.[13,14] All these ways to produce orientation are based on the interaction of electric fields with the charge density of the molecule, requiring reagents with permanent dipole moments. This is the reason why some of the experiments were devoted to reactions between alkali and halides where reactants and products present strong dipole moments.[15]

Among these systems Li + HF→ LiF + H is one of the candidates and some stereodynamical studies have already been done experimentally. Loesch and coworkers produced the excitation of HF using linearly polarised laser generated in a crossed beam experiment.[12,14,16–18] Because the transition is parallel, HF is excited to $v = 1$, $j = 1$, $m = 0$. When the polarization axis of the field changes the molecule can be aligned either parallel or perpendicular to the relative velocity vector **k**. A weak homogeneous field was added along the centre-of-mass motion to avoid the depolarization induced by hyperfine couplings. The values obtained for the integral cross section (ICS) and DCS show important steric effects, favouring a side attack. Some extra ICS measurements have been done by Lee and co-workers[19] and Loesch and co-workers.[20–22]

The steric effects have also been analyzed theoretically for an initial excitation of HF to $v = 1$, $j = 1$ using quantum[23] and quasi-classical theory (QCT).[18,24,25] It has been analyzed by using the stereodirected representation for $J = 0$[26,27] and $J = 1$ and 10.[28,29] These results present good agreement with the experiments.[12,14,16] Experiments and calculations show that the initial vibrational excitation of HF, even by only one quantum, increases reactivity dramatically.[12,16,18,23] This effect is concluded to be due to the late character of the reaction barrier. Another effect obtained in the simulations is the dependence of the reaction on the helicity for initial $v = 0$, while for $v = 1$ it does not play a significant role. The reason for that is that in collinear collisions the vibrational excitation of reactants is favoured, which is needed for $v = 0$ because of the late barrier character of this reaction.

The reaction Li + HF → LiF + H is considered a benchmark of the alkali + halide type of reaction since it is the lightest of this kind. This allows reliable potential energy surfaces (PES) for the ground state[30–33] as well as for the excited states.[34,35] There are many theoretical simulations of the reactive collision for this reaction including QCT,[18,22,36,37] time independent (TI) quantum dynamics[29,31,38–41] and time-dependent wave packet (WP) calculations.[23,42–46] The experimental stereodynamic results have motivated many theoretical simulations as well.[23–28,32] More recently all these studies were extended to ultracold temperatures.[47,48]

Despite all these theoretical studies, DCSs have only been calculated using the QCT approach,[22] and just recently quantum mechanical calculations were done for Li + HF($v = 0, j = 0$). The appearance of many resonances and zero point effects in this reaction suggests that the quantum mechanical simulations of DCS are the most adequate way to mimic experimental results. For this reason we have decided to extend the quantum simulations to higher rotational states and analyse the effect of reactant polarization in the DCS.

The paper is structured as follows. Section II is devoted to describing the theoretical treatment. Since pioneering work published by Case and Herschback[1] many other vector correlation treatments have been proposed[24,25,49–51] but a brief outline is presented here for clarity. In section III, the results obtained for Li + HF → LiF + H are described and discussed. Finally, section IV is devoted to extracting some conclusions.

II. Theoretical treatment

The wave function describing AB(v,j,m) + C → A + BC(v',j',m') reactive collisions, for an energy E and long distances between products, $R' \to \infty$, in a reference system where the z-axis is parallel to the initial velocity vector between reactants, **k**, is expressed as

$$\Psi_{vjm}(\hat{k}', E) \underset{R'\to\infty}{\propto} \sum_{v'j'm'} F_{vjm,v'j'm'}(\hat{k}', E)\frac{e^{ik'_{v'j'}R'}}{R'}\frac{\varphi_{v'j'}(r')}{r'}Y_{j'm'}(\hat{r}') \tag{1}$$

where standard product Jacobi coordinates r', R', γ' are used, and v',j',m' (v,j,m) denotes the product (reactant) quantum numbers for vibration, angular momentum and its projection in the reactants body-fixed (BF) frame. Hereafter, prime (unprimed) quantities are referred to as products (reactants). $\mathbf{k}'$ is the wave vector in the products channel v',j', of norm $k'_{v'j'} = \sqrt{2\mu'(E - E_{v'j'})/\hbar^2}$. $E_{v'j'}$ and $\varphi_{v'j'}(r')$ are the rovibrational eigenvalues and eigenvectors of BC(v',j',m') fragments, and $\mu' = m_A(m_B + m_C)/(m_A + m_B + m_C)$ the reduced mass.

The final rotational states of the products can be transformed to the body-fixed frame of products, in which the z'-axis is parallel to $\mathbf{k}'$, through a rotation

$$Y_{j'\Omega'}(\hat{r}'_{bf}) = \sum_{m'} Y_{j'm'}(\hat{r}')D^{j'}_{m'\Omega'}(\hat{k}')$$

$$Y_{j'm'}(\hat{r}') = \sum_{\Omega'} D^{j'*}_{m'\Omega'}(\hat{k}')Y_{j'\Omega'}(\hat{r}'_{bf}),$$

where m', Ω' are the projections of angular momentum $\mathbf{j}'$ in the z-axes of reactants and products body-fixed frames, respectively. Using these expressions in eqn (1), the asymptotic collisional eigenfunction becomes

$$\Psi_{vjm}(\hat{k}', E) \underset{R'\to\infty}{\propto} \sum_{v'j'\Omega'} f_{vjm,v'j'\Omega'}(\hat{k}', E)\frac{e^{ik'_{v'j'}R'}}{R'}\frac{\varphi_{v'j'}(r')}{r'}Y_{j'\Omega'}(\hat{r}'_{bf}). \tag{2}$$

In eqn (1) and (2), F and f are the collision amplitudes, and the relationship between them is

$$\begin{aligned} F_{vjm,v'j'm'}(\hat{k}', E) &= \sum_{\Omega'} D^{j'}_{m'\Omega'}(\hat{k}')f_{vjm,v'j'\Omega'}(\hat{k}', E) \\ f_{vjm,v'j'\Omega'}(\hat{k}', E) &= \sum_{m'} F_{vjm,v'j'm'}(\hat{k}', E)D^{j'*}_{m'\Omega'}(\hat{k}'). \end{aligned} \tag{3}$$

For a coherent superposition of initial rotational states and a coherent detection of products rotational levels, it is interesting to define a generalized cross section as[24,50–52]

$$\sigma_{vjm_1m_2\to v'j'm'_1m'_2}(\hat{k}', E) = F^*_{vjm_1,v'j'm'_1}(\hat{k}', E)\,F_{vjm_2,v'j'm'_2}(\hat{k}', E). \tag{4}$$

Describing the initial superposition of rotational states by the density matrix $\rho^{vj}_{m_1,m_2}$, the DCS is obtained as[53]

$$\sigma_{vj\to v'j'm'_1m'_2}(\hat{k}',E)=\sum_{m_1,m_2}\rho^{vj}_{m_1,m_2}\sigma_{vjm_1m_2\to v'j'm'_1m'_2}(\hat{k}',E) \quad (5)$$

Thus for an incoherent isotropic distribution, the standard $v,j \to v',j'$ state-to-state DCS is defined by setting $\rho^{vj}_{m_1,m_2}$ diagonal with diagonal matrix elements equal to $(2j+1)^{-1}$, resulting in

$$\begin{aligned}\sigma^0_{vj\to v'j'}(\hat{k}',E) &= \frac{1}{2j+1}\sum_{m,m'}|F_{vjm,v'j'm'}(\hat{k}',E)|^2\\ &= \frac{1}{2j+1}\sum_{m,\Omega'}|f_{vjm,v'j'\Omega'}(\hat{k}',E)|^2.\end{aligned} \quad (6)$$

A. State multipoles and multipole moments

Instead of calculating the cross section for each initial density matrix, it is more convenient to expand $\rho^{vj}_{m_1,m_2}$ over the state multipoles.[1,49,54] The state multipoles are spherical operators[53,55] defined as

$$\hat{t}^{(j)}_{KQ}=\sum_{m_1,m_2}(-1)^{j-m_2}\sqrt{2K+1}\begin{pmatrix} j & j & K\\ m_2 & -m_1 & -Q\end{pmatrix}|jm_2\rangle\langle jm_1|, \quad (7)$$

and the coefficients of the expansion, or multipole moments, are defined as[54]

$$\rho^{vj}_{KQ}=\sum_{m_1,m_2}(-1)^{j-m_2}\sqrt{2K+1}\begin{pmatrix} j & j & K\\ m_2 & -m_1 & -Q\end{pmatrix}\rho^{vj}_{m_1,m_2} \quad (8)$$

A density matrix describing the superposition of final states of products can be defined by re-normalizing the DCS for an arbitrary superposition of initial states, eqn (5), as

$$\rho^{v'j'}_{m'_1m'_2}(\hat{k}',E)=\sigma_{vj\to v'j'm_{1'}m_{2'}}(\hat{k}',E)/\sigma^0_{vj\to v'j'}(\hat{k}',E). \quad (9)$$

Thus, it can also be expanded in state multipoles, whose multipole moments are given by an expression analogous to eqn (8) but replacing all the quantum numbers by their analogue for products, which are primed. This normalization in eqn (9) is set to describe the polarization of products for each energy E and direction $\mathbf{k}'$ independently.

According to eqn (8) and (9) the $K'=0$ multipole moment is normalized to $(2j'+1)^{-1/2}$. The $K'=1,2$ and $Q'=0$ state multipole moments are given by:

$$\begin{aligned}\rho^{v'j'}_{10} &= \sum_m\frac{m'}{\sqrt{j'(j'+1)(2j'+1)}}\rho^{v'j'}_{m',m'}\\ \rho^{v'j'}_{20} &= \sum_m\frac{3(m')^2-j'(j'+1)}{\sqrt{j'(j'+1)(2j'+3)(2j'+1)(2j'-1)}}\rho^{v'j'}_{m',m'}\end{aligned} \quad (10)$$

which are proportional to the known rotational orientation and alignment parameters[56]

$$\begin{aligned}\mathcal{O}^{v'j'}_{Q'=0}(\hat{k}',E) &= \sum_{m'}\left[\frac{m'}{\sqrt{j'(j'+1)}}\right]\rho^{v'j'}_{m'm'}(\hat{k}',E)\\ \mathcal{A}^{v'j'}_{Q'=0}(\hat{k}',E) &= \sum_{m}\left[\frac{3(m')^2}{j'(j'+1)}-1\right]\rho^{v'j'}_{m'm'}(\hat{k}',E),\end{aligned} \quad (11)$$

defined with respect to the z-axis parallel to $\mathbf{k}$ in the reactants frame.

The same coefficients can be defined with respect to products frame, in which the projections on z'-axis, Ω', will be used instead of m' in the results section.

Thus, when the orientation $\mathcal{O}_{Q'=0}$ approaches $+1$ (or -1), the most probable event corresponds to $\mathbf{j}'$ pointing in the same (opposite) direction as $\mathbf{k}$. If the quantization axis is taken along $\mathbf{k}$ and an initial isotropic distribution is assumed, the orientation and all odd terms of the multipole expansion vanish for $Q'=0$. In photodissociation, the asymmetry is introduced by circularly polarized light, so that integral and differential[54] cross sections can be different from zero. For $Q'\neq 0$, however, out of the scattering plane, $\mathcal{O}_{Q'\neq 0}$ can be different from zero even in the case of excitation by linearly polarized light.[54] The alignment $A_{Q'=0}$ is generally non-zero and takes the limiting values of -1 and 2, depending on whether $\mathbf{j}'$ is perpendicular or parallel to $\mathbf{k}$, respectively.

B. Collision amplitude and S-matrix

The collision amplitudes $f_{vjm,v'j'\Omega'}(E,\hat{k}')$ are obtained from the collision S-matrices as[57–59]

$$f_{vjm,v'j'\Omega'}(E,\hat{k}')=\frac{1}{2k_{vj}}\sum_J(2J+1)\times S^J_{vjm,v'j'\Omega'}(E)\,d^J_{m\Omega'}(\Theta), \quad (12)$$

where $d^J_{m\Omega'}(\Theta)$ are reduced Wigner rotation matrices[56] depending on the center of mass (CM) scattering angle Θ, the polar angle vector of $\mathbf{k}'$. J is the total angular momentum. The scattering amplitude entirely expressed in reactants body-fixed frame, $F_{vjm,v'j'm'}(E,\hat{k}')$, is directly obtained using eqn (12) and (3).

The procedure used to obtain the S-matrix elements can be summarized as follows:

1. The overlap between the $|v'j'\Omega'\rangle$ product state (where Ω' is a helicity component) and the kth Chebyshev iteration of the wavepacket $\Phi^{J\varepsilon}_{\Omega'}(k)$, using a modified Chebyshev propagator[60–65] to integrate the Schrödinger equation, is evaluated at $R'=R'_\infty$ as

$$C^{J\varepsilon}_{vjm\to v'j'\Omega'}(k)=\int\sin\gamma'\mathrm{d}r'\mathrm{d}\gamma'\varphi_{v'j'}(r')\,Y_{j',\Omega'}(\gamma',0)\langle r',R'_\infty,\gamma'|\Phi^{J\varepsilon}_{\Omega'}(k)\rangle, \quad (13)$$

for each total angular momentum J and a parity ε under inversion of spatial coordinates. These coefficients are directly obtained by numerical integration using product coordinates in the propagation. When using reactant coordinates, however, a reactant-to-product transformation must be done, at each

iteration k, which could be very demanding computationally. Here, this transformation is done using an efficient transformation method recently proposed.[66]

2. The quantity in eqn (13) is transformed to the energy domain as[65,67]

$$C^{J\varepsilon}_{vjm\to v'j'\Omega'}(E) = \sum_k c_k(\hat{H}_s, E) C^{J\varepsilon}_{vjm\to v'j'\Omega'}(k) \qquad (14)$$

where $\hat{H}_s = (\hat{H}-E_0)/\Delta$ is the energy scaled Hamiltonian used in the Chebyshev propagation (with $E_0 = (E_{\max}+E_{\min})/2$, $\Delta = (E_{\max}-E_{\min})/2$) and

$$c_k(\hat{H}_s, E) = \frac{(2-\delta_{k0})\hbar e^{-ik\arccos(E-E_0)/\Delta}}{\sqrt{\Delta^2-(E-E_0)^2}}. \qquad (15)$$

3. $C^{J\varepsilon}_{vjm\to v'j'\Omega'}(E)$ coefficients, with $\Omega' \geq 0$, and parity under spatial inversion $\varepsilon = \pm 1$, are transformed from products body-fixed frame to space-fixed (SF) frame as

$$Q^J_{v,j,\ell\to v',j',\ell'}(E) = \sum_{m\geq 0}\sum_{\Omega'\geq 0}^{J} T^{J\varepsilon j}_{m,\ell}\, C^J_{v,j,m\to v',j',\Omega'}(E)\, T^{J\varepsilon j'}_{\Omega',\ell'}, \qquad (16)$$

where the sum over m and Ω' runs only for positive values, and

$$T^{J\varepsilon j}_{\Omega',\ell} = \sqrt{2-\delta_{\Omega'0}}\,(-1)^{j-\ell-\Omega'}\sqrt{2\ell+1}\begin{pmatrix}\ell & j & J\\ 0 & \Omega' & -\Omega'\end{pmatrix} \qquad (17)$$

are the SF-to-BF transformation matrix elements. This transformation matrix is usually applied to transform wave functions. When dealing with S-matrix there is an extra phase factor $i^{\ell'-\ell}$ which appears.[57–59] In the present treatment, this factor cancels because this transformation is applied twice, once in step 3 and a second time backward in step 5 below.

4. The S-matrix in the space-fixed reference system is obtained as

$$S^{J\varepsilon}_{v,j,\ell\to v',j',\ell'}(E) = -i\sqrt{\frac{2k_{v'j'}}{\pi\mu'}}\frac{1}{a_{vj\ell}(E)}\frac{e^{-i\ell'\pi/2}}{h^{(2)}_\ell(k_{v'j'}R'_\infty)}Q^{J\varepsilon}_{v,j,\ell\to v',j',\ell'}(E) \qquad (18)$$

where $h^{(2)}_\ell(x)$ are spherical Bessel functions of the third kind. Here, the energy distribution of the initial wave packet, $a_{vjm}(E)$, is obtained as

$$a_{vj\ell}(E) = \frac{1}{2i}\sqrt{\frac{\mu}{2\pi\hbar^2 k_{vj}}}\int dR\, e^{ik_{vj}R} g^{Jvj\ell}(R, t=-\infty) \qquad (19)$$

where $g^{Jvj\ell}(R,t=-\infty)$ is the result of propagating back in time the initial Gaussian function, using a centrifugal barrier $\ell(\ell+1)/2\mu R^2$. This propagation allows a better determination of the energy distribution of the initial wave packet from a relatively short distance, where the potential is negligible but the centrifugal barrier is still important for high ℓ.

5. Finally, S-matrix elements are obtained by a transformation back from the SF frame to the BF frame as

$$S^J_{v,j,m\to v',j',\Omega'} = \sum_\ell\sum_{\ell'} T^{Jj}_{\Omega',\ell}\, S^J_{v,j,\ell\to v',j',\ell'}(E)\, T^{Jj'}_{\Omega',\ell'}, \qquad (20)$$

where the new transformation now reads

$$T^{Jj}_{\Omega',\ell} = (-1)^{j-\ell-\Omega'}\sqrt{2\ell+1}\begin{pmatrix}\ell & j & J\\ 0 & \Omega' & -\Omega'\end{pmatrix} \qquad (21)$$

and runs for positive and negative Ω' values, since non-parity adapted BF functions are used to represent the S-matrix.

With this procedure, the S-matrix elements are obtained as required in eqn (12).

III. Results and discussion

In this work wave packet calculations have been performed for Li + HF(v = 0, j = 1, 2 and 3) → LiF(v',j') + H for J = 0,1,2,...,45 for m = 0,...,min(j,J) and the two parities under coordinate inversion, $\varepsilon = \pm 1$. The propagation in time has been done using a modified Chebyshev integrator[60–65] using reactant Jacobi coordinates in a body-fixed frame. At each iteration, a transformation to product Jacobi coordinates is done to analyze the final flux on different LiF(v',j') channels, using an efficient method described in ref. 66. The MAD-WAVE3 program has been used for doing the calculations.[50]

The parameters used in the wave packet propagation are the same as those used in ref. 50 for the initial case of j = 0. Briefly, the grids used are determined by the convergence of state-to-state reaction probabilities for J = 0 to be better than 0.1%. The number of helicity components is set to a maximum of 16 functions ($\Omega_{\max}$ = min(J,15)), yielding DCSs which are in good agreement with the same results obtained with 32 functions (better than 0.1%), as studied for Li + HF(v = 0, j = 0).[50] Finally the number of Chebyshev iterations used is of the order of 20 000. This number was checked to converge rotational average state-to-state probabilities to values better than 1%, in most of the energy intervals considered. This high number is necessary to get convergence for narrow resonances, typically appearing at low J. For higher J values, the resonances disappear and the number of iterations can be reduced to 10 000, which is done here for $J > 35$.

The APW PES by Aguado *et al.*[68] has been used in the present case. The minimum of the HF potential well at the asymptote has a lower energy than the LiF one, but when zero-point energy effects are included the situation changes to the opposite situation, becoming exoergic by −0.08 eV. In the entrance channel there is a well of ≈−0.25 eV, corresponding to the Li-HF complex. In addition, the system presents a late barrier, *i.e.* a reaction barrier in products channels for an elongated HF distance of r_{TS} = 1.2682 Å. This barrier is the result of a curve crossing between a covalent and ionic electronic states, correlating with Li(^2S) + HF($^1\Sigma^+$) and $Li^+(^1S)$ + HF^-.[35] The main features of this PES are summarized in Fig. 1, and are very similar to those previously reported and discussed in detail.[23,32]

A. Reaction probabilities for J = 0 and integral cross section

Total and vibrational reaction probabilities for the Li + HF(v,j) → LiF(v') + H collisions are presented in Fig. 2, for zero total angular momentum, J = 0. The results are qualitatively similar to those obtained with a different PES,[23,32] and will be described briefly here.

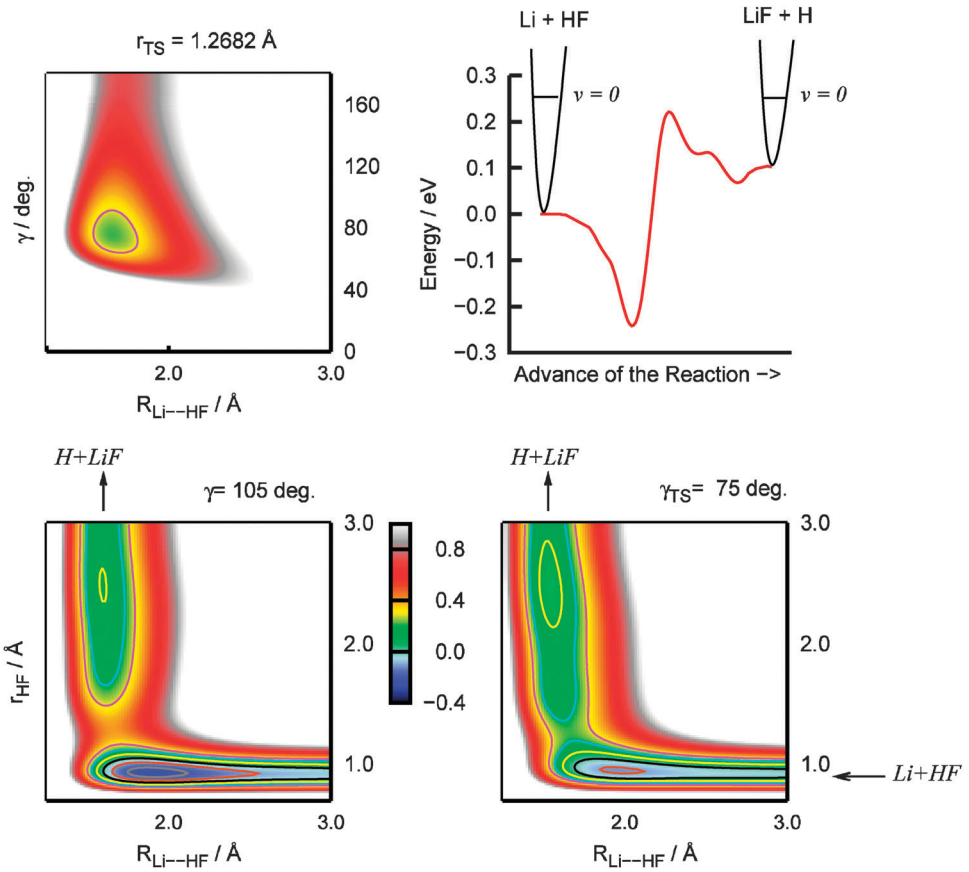

Fig. 1 Minimum energy path and contour plots of the Li-HF PES of ref. 68 (top-right panels), and different two-dimensional cuts of the PES to show the late character of the barrier at $\gamma = 75°$ (bottom right panel), the well in the entrance channel at $\gamma = 105°$, and the saddle point at $r_{HF} = 1.2682$ Å.

The reaction probability for $v = 1$ is much higher than for $v = 0$. Moreover, summing over the partial waves, the integral reaction cross sections presents a larger difference.[12,16,18,23] The vibrational energy difference is $\approx$0.5 eV, so that the total energy for a collisional energy 0.5 is the same as that for $v = 1$ and $E_c = 0$. The reason for this difference is not the total energy, but the initial vibrational excitation of the reactants, which does not seem to be easily transferred as otherwise there would not be such large differences between the corresponding reaction probabilities. This situation is due to the late barrier character of the reaction, corresponding to an elongated HF distance. This barrier is more easily overcome when there is some vibrational excitation, while translational excitation does not help, as predicted by Polanyi's rules.[69,70]

The reaction probabilities for $v = 0$ but different j values are rather similar, showing two regions, one below $\approx$0.15 eV, dominated by resonances attributed to the Li-HF well in the entrance channel, and the higher energy interval, in which the total probabilities are smooth but the vibrationally resolved probabilities show broad oscillations. All the narrow structures appearing at low energies were attributed to resonances supported by the well in the entrance channel, corresponding to the Li-HF complex, and have been analyzed before for different PESs.[23,31,38,71] Their energies are below the reaction barrier, or just above it because the reaction threshold is increased by the zero-point energy at the saddle point. These resonances can only decay on the products channel by tunneling through the barrier. For this reason, these tunneling resonances are rather narrow.

Above 0.15 eV, the vibrationally resolved probabilities show broad oscillations, which were attributed to interference effects[31] or to transition state (TS) resonances above the barrier.[23] This last case was justified as follows. Freezing the HF distance (the reaction coordinate) at the saddle point, the PES shows a well (see Fig. 1). This well presents bound states, which coincide approximately with the maxima of the oscillations of the reaction probability.[23] These TS resonances are very broad because they are immersed in the dissociative continua of reactants and products channels. As energy increases, the vibrational spectrum of the TS becomes more congested and the oscillations tend to disappear.

The final rotational distribution, in Fig. 3, is very structured, showing all the resonant structure. For low final rotational excitations, even values of j' have a population significantly higher than those obtained for odd j values. For higher j values this difference decreases. Such difference indicates a net separation between even/odd j' dynamics, which has already been observed.[45] This was interpreted by the features of the transition state region.

The TS is ionic, corresponding to a bent Li^+F^-H, because the reaction barrier is created by a covalent/ionic crossing,[35] in which an electron "jumps" from the Li atom to the F atom in the-so called harpoon mechanism. The HF^- subunit created

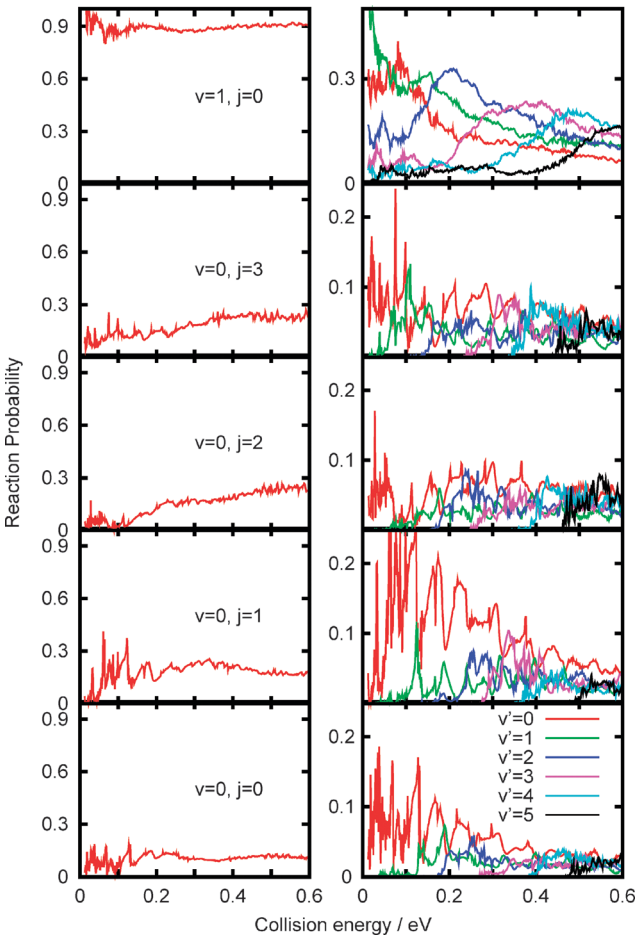

Fig. 2 Total (left panels) and vibrationally resolved (right panels) reaction probabilities for the Li + HF(v = 0,j) → LiF(v') + H for v = 0, j = 0,1,2,3 and v = 1, j = 0, with total angular momentum J = 0.

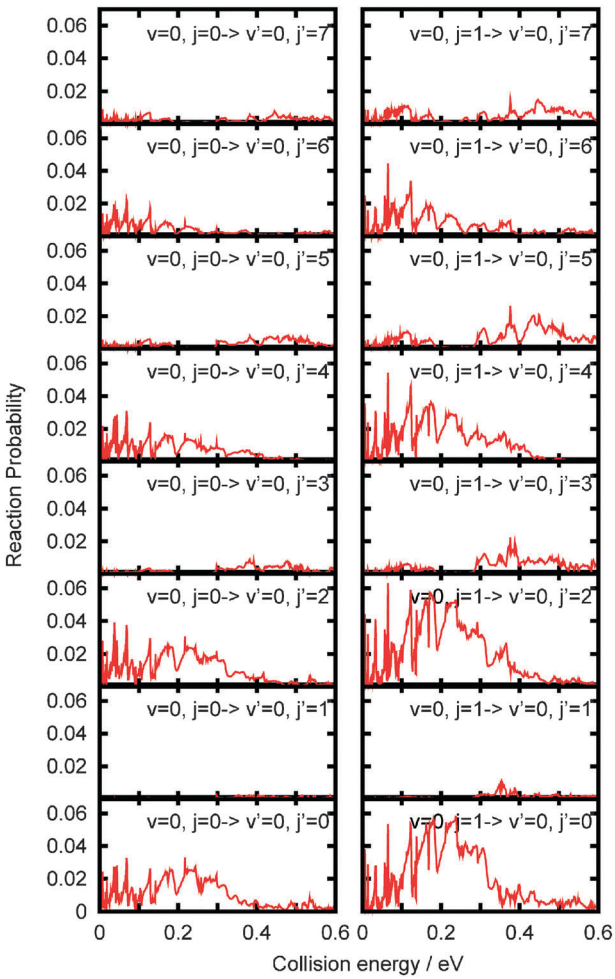

Fig. 3 Rotationally resolved reaction probabilities for the Li + HF(v = 0,j) → LiF(v') + H for v = 0,j' and total angular momentum J = 0. Results for j = 0 and 1 are shown in the left and right panels, respectively.

corresponds to a non-bonded system which shows a dissociative potential with no wells, and at the equilibrium distance of neutral HF the system is placed in a very repulsive region. Hence, once the barrier is overcome, the H atom dissociates quickly due to the HF^- repulsive interaction, leaving the strongly attractive Li^+F^- ionic products. This is the so-called direct interaction with product repulsion (DIPR) mechanism, recently reviewed,[72] typical of metal atom (M) with hydrogen halide (HX) reactions: the electron jumps from M forming HX^- transient, which is unstable and dissociates rapidly, leaving the M^+X^- ionic products. The fast dissociation means that the features of the distribution of products are determined by the transition state region.

Maintaining the argument above in mind, it is important to note that the bent saddle point, expressed in LiF–H Jacobi coordinates, corresponds to an angle $\gamma' \approx \pi/2$. Assuming a local harmonic behavior of the potential, TS state resonances correspond to either odd or even eigenstates with respect to $\gamma' \rightarrow \pi-\gamma'$ symmetry. Thus these states, mediating the reaction dynamics, dissociates rapidly keeping the even/odd separation. This simple model would explain the even/odd final state distribution obtained for J = 0, with Ω' = 0.

For Ω' = 1, even/odd j values correspond to antisymmetric/symmetric, the opposite to the case of Ω' = 0. In this case the ground rotational state is j' = 1. Thus, each Ω' manifold will present a different sequence of transition state resonances, whose ground state has a major contribution from the $j' = \Omega'$. When summing over all partial waves and helicities, Ω', the even/odd alternation of the rotational population is washed out.

The total integral reaction cross sections, shown in the left panels of Fig. 4, can also be divided in two regions. In the low energy part, up to ≈0.1–0.2 eV for j = 0, the cross section show several peaks, which arise from the summation of the resonant structures at each partial wave. Thus, the individual traces of resonances are lost. The narrow tunneling resonances appearing at each J group together, forming new broader structures (for $E_c < 0.1$–0.2 eV). This could be the reason why the quasi-classical results of ref. 22 are so smooth. In addition, since classically there is no zero-point energy at the transition state, the reaction has classically no threshold, and the corresponding cross section should decrease with increasing energy.

In the high energy range, the quantum results show oscillations, associated with the TS resonances. Classical and quantum results are of the same order of magnitude, and seem to get closer as energy and j increase. As j increases, the overall magnitude of the cross section do not change strongly.

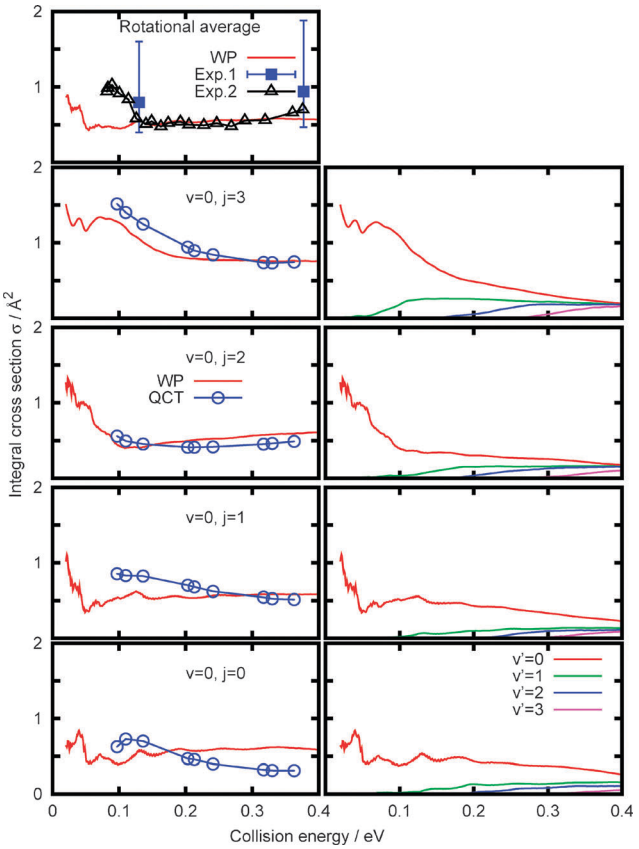

Fig. 4 Total (left panels) and vibrationally resolved integral cross section for the Li + HF(v = 0,j) → LiF(v') + H. The QCT results are from ref. 22 and represented by open circles. The rotationally averaged cross section is compared with the experimental results from ref. 19 and ref. 20. The rotational average is built with the rotational populations at the stagnation conditions of 315 K measured in ref. 22. Note that the results of ref. 20 are in arbitrary units, and rescaled here for comparison.

The value of the cross section at 0.4 eV is very similar for all j values studied. However, at low energies it changes gradually from ≈0.5 Å^2 for j = 0 to 1.5 Å^2 for j = 3. This behaviour is interpreted as follows: at low translational energies the increase of rotational excitation allows the system to explore the PES near the bent transition state. As translational energy increases, the rotational excitation becomes negligible and the effect disappears.[23]

The results obtained are between the error bars of the measurements of the absolute cross section of Becker *et al.*,[19] which have large error bars. The experimental results reported by Höbel *et al.*[20] are in arbitrary units and were rescaled. The overall agreement between these last experimental measurements and theoretical results is reasonable, except in the fast increase of the experimental cross section at E_c = 0.1 eV, which in the quantum calculations appear at lower energies. This low energy part depends strongly on details of the barrier height and of the long range interaction potential, and the disagreement seems to indicate that there may be some inaccuracies in the PES. The exact position of tunneling resonances determining these fast increases depend strongly on the shape of the PES in a large region of the configuration space.

The increase of the experimental cross section[20] observed for energies below 0.12 eV is in surprisingly good agreement with the results obtained theoretically for j = 3. The theoretical average was performed using the rotational populations determined experimentally at the stagnation conditions of 315 K.[22] This population corresponds to a rotational temperature of 70 K, in which the population of j = 3 is only 2.7%. Increasing the temperature would increase the weight of high j, getting a better agreement with the experimental results.[20] The "exact" quantum calculation of higher j values is very demanding computationally, and should probably be addressed using quasi-classical methods.

The vibrationally resolved cross sections, in the right panels of Fig. 4, show the progressive opening of the excited vibrational levels. At low energy only v' = 0 is open and the cross section is very structured. These structures are associated with tunneling resonances because the reaction probabilities showed many peaks at the same energies associated with resonances, as discussed for J = 0. As commented above, for j = 0 the reaction presents a reaction threshold, below which the reaction can only take place through tunneling. Reactions with thresholds typically show an increase followed by a decrease in the reaction cross section. For higher j values, however, the threshold shifts toward lower energies, or disappears, because the rotational energy of the reagents increases. In the absence of a threshold, the cross section tends to decrease as collision energy increases.[73]

For E_c > 0.1 the first excited vibrational states open. Since these energies are considerably higher than the reaction threshold due to the zero-point energy at the saddle point, the cross section for v' > 0 are smoother, with an increase as the channel opens, followed by a slow decrease which only shows very broad oscillations associated with the TS resonances. It is interesting that for higher collision energies considered here, all product vibrational levels become equally populated. Moreover, at these higher energies, the relative weight of the v' = 0 state decreases with increasing initial j. This may imply that initial translational and rotational energy transforms in vibrational energy of products, because of the late barrier character of the reaction and the skewing angle of this reaction. This is again explained by Polanyi's rules: in late barrier reactions reactant translational energy transforms into vibrational energy of products.

B. Effect of the polarization of reactants

The dependence of the reactivity on the rotational orientation, or **k**–**j** correlation, can be obtained from the cross section for selected initial helicity quantum number m, and it is shown in Fig. 5. If the Coriolis coupling does not strongly mix different m values, the mutual **k**–**j** orientation does not change. This is the case for the Li + HF reaction, for which centrifugal sudden approach is rather satisfactory for the total cross section.[32] The reason is that the reactant Jacobi vector, **R**, nearly coincides with one of the inertia axes, because the light H atom is close to the heavier F atom in the entrance channel. In the products channel, however, when H gets far from the heavier atoms, this approximation gets worse, and Coriolis coupling is more efficient. For this reason, it is expected that the centrifugal sudden approach is going to work worse for state-to-state magnitudes.

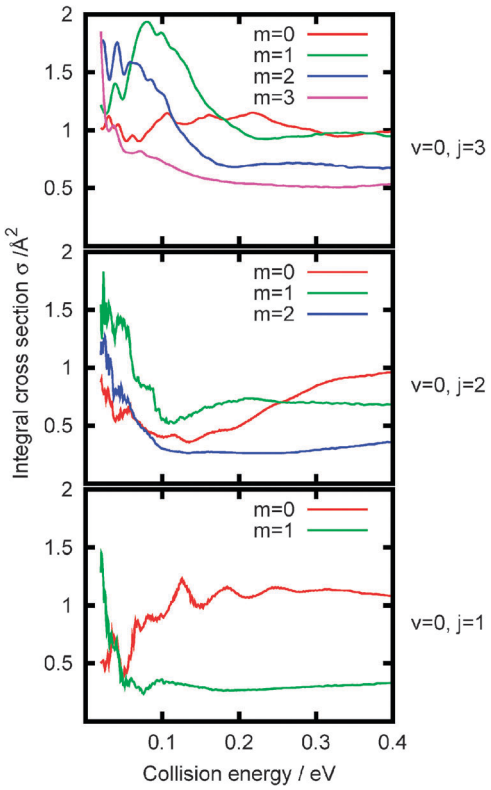

Fig. 5 Integral cross section for the Li + HF($v = 0,j$) reaction for different initial helicities, m. For $m < 0$ the cross sections are nearly the same as for $|m|$, the largest differences being at low energies (below 0.1 eV) where the tunneling resonance contribution is large.

Since m may be considered to be conserved in the entrance channel up to the saddle point, we can consider as a crude approach that the initial **k**–**j** relative geometry is maintained in the entrance channel until reaching the reaction barrier. Asymptotically **k** is parallel to the z body-fixed axis, and the HF internuclear vector, **r**, is in the x–z body fixed plane. For $m = 0$, **j** and **k** are mostly perpendicular, and **r** and **k** are parallel. For $m = j$, **j** and **k** are mostly parallel, and **r** and **k** are perpendicular. In the case of the title reaction, there is a strong dependency of the cross section with m, as can be seen in Fig. 5. This result indicates that the Coriolis coupling is not strong enough to produce a complete randomization among the different helicities in the entrance channel, so that the m-dependence (or **j**–**k** correlation) is preserved.

For $j = 1$, the cross section for $m = 0$ is clearly larger than for $m = 1$, demonstrating that the reaction occurs preferentially at collinear geometries, when using the body-fixed frame used for studying the dynamics. In other words, the cartwheel collision geometry is preferred to the propeller one, in the space fixed frame. For $j = 2$, $m = 2$ appears the smallest cross section, while $m = 1$ is the largest for low energy, and $m = 0$ for high collision energies. This suggests that for strictly collinear collisions, the reactants would rebound back without reaching the TS. A slightly bent collision geometry is then necessary to get both a vibrational excitation and a bent geometry which drives the system towards the bent and late barrier configuration. The results obtained for $j = 3$ are analogous: $m = 0$ and 1 yields larger cross sections, and their relative importance varies with energy, while the largest m gives rise to the smaller cross section.

These results are in agreement with previous results obtained with another PES.[23] Those results were obtained in the centrifugal sudden (CS) approximation, in which m is fixed along the reaction dynamics. In the present work, m can vary because the Coriolis coupling is not neglected. Thus, the fact that the reaction cross section has a strong dependence on the initial m means that the Coriolis coupling in the entrance channel does not randomize the helicity m values. In such a situation all m would yield a similar reaction probability. We conclude that the centrifugal sudden approach assumed in ref. 23 is rather good in the entrance channel, *i.e.* until the system has overcome the saddle point. After this point, the helicities can mix strongly without affecting to integral cross sections.

The fact that the reaction depends so strongly on the initial helicity m indicates that the angular cone of acceptance is rather narrow in these cases of $v = 0,j$. For $v = 1$, however, it was found[23] that the reaction cross section is considerably larger and that it does not depend on the initial m. Since in that case the CS approach was used (and should also be a good approximation), the only explanation is that the angular cone of acceptance in that case is considerably larger. This situation holds for all the collision energies studied,[23] from 0 up to 0.5 eV. However, at the same total energies, when starting at $v = 0$, the situation is completely different showing the strong dependence on the initial m described above.

This difference between $v = 0$ and $v = 1$ dynamics can then only be understood by an energy separation between the motion along the reaction coordinate and along the two perpendicular degrees of freedom. The reaction barrier has a late character, corresponding to a relatively long HF internuclear distance, r. At this point the reaction coordinate is parallel to r, as shown in Fig. 1. For $v = 0$, the energy along the reaction barrier is low, and the dynamics is determined by the TS resonances and by a narrow angular cone of acceptance, around the $\gamma_{TS} = 105°$. This angle would imply that the most probable initial helicity should be $m = j$, for which the reactant Jacobi vectors **r** and **R** are perpendicular. The fact that, on the contrary, the higher reactivity is found for $m = 0$ or 1, suggests that the mechanism is slightly more complicated.[23] The HF vibrational excitation determines whether the system can overcome the reaction barrier. In the case of $v = 1$, the excitation is enough to overcome the barrier and for this reason the reaction cross section does not depend on the initial m. On the contrary, for $v = 0$ there is not enough energy along the reaction coordinate. The vibrational excitation needed is essentially acquired in Li + HF nearly collinear collisions, while for perpendicular collisions the translational energy is more probably transferred to HF rotation. Quantum studies performed for selected J values using the so-called sterodirected representation also find that the reaction is more probable for angles corresponding to nearly collinear geometries[26–29] If the collision is strictly collinear, HF would be very excited but it would rebound back without finding the bent TS. This explains why not only $m = 0$ is important but also $m = 1$, *i.e.* not strictly collinear geometries are the most effective for producing the

reaction: a sufficiently bent geometry is needed to get the system bent after getting enough HF excitation to overcome the late reaction barrier.

This was also corroborated by simulations of the infrared excitation of the van der Waals Li–HF complex, in which a single HF vibrational quantum was enough to produce the reaction.[74]

C. Differential cross section and polarization of reactants

The total DCS for the title reaction and for an initial isotropic rotational distribution of the HF reactant are shown in Fig. 6, and they are compared for $v = 0$, $j = 0$ with quasi-classical results of ref. 22. The DCS is asymmetric with several peaks in all cases. There is nearly always forward and backward (0 and 180° respectively) peaks, whose relative differences depend on the initial j and the collision energy. Also, side scattering is always important, showing a rather complicated structure. It is difficult to rationalize the DCS because it shows a rather different behavior as a function of energy and j. For low energies the DCS for all j values are significantly different, and the back-scattering peak seems to be favoured for high j, probably because the system has enough time to rotate during the collision. As collisional energy increases, the DCS obtained

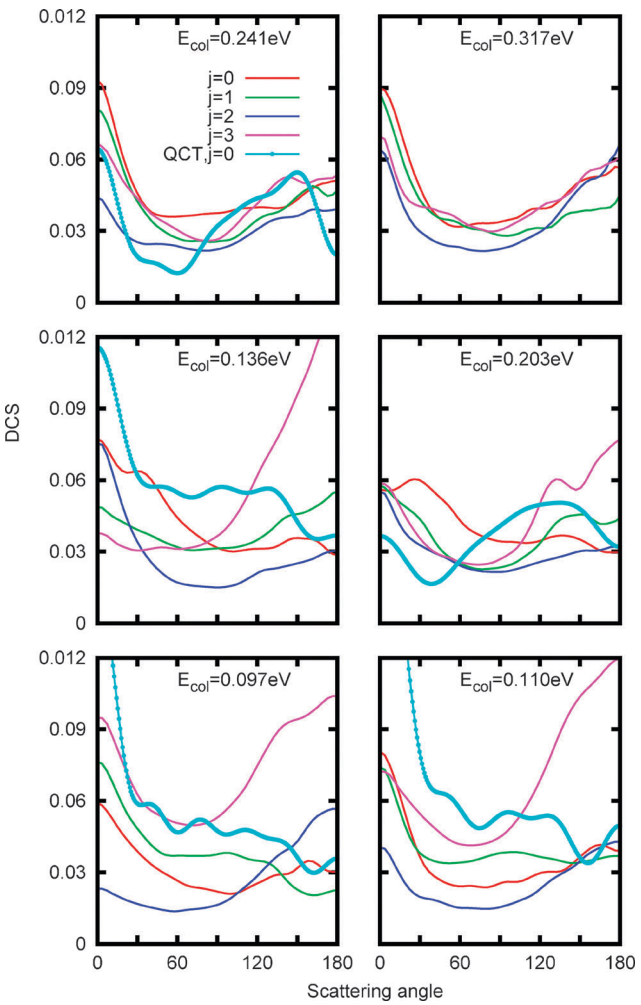

Fig. 6 Total differential cross section for different energies and for $v = 0$, $j = 0$,1,2 and 3. The QCT results are from ref. 22.

for different j values become gradually more similar. For the highest energy considered, $E = 0.317$ eV, all the DCSs are very similar, and the forward scattering becomes higher. As discussed above, tunneling (up to 0.1 eV) and TS resonances play an important role in the dynamics, especially for lower energies. These resonances could explain the distinct behavior of the DCS for different j and energies. As energy increases, tunneling resonances do not contribute and TS resonances manifest differently for each v'. Thus, the effect of resonances as energy increases is expected to wash out for high energies, especially when considering that the number of partial waves also increases. The strong dependence of quantum results on j and energy, attributed to resonances, explains the differences obtained with quasi-classical results.

A deeper insight is obtained by examining the vibrationally resolved Li + HF(v,j,m) → LiF(v') + H, for different v' and different initial values of m, as shown in Fig. 7. For $j = 1$, the DCS for $m = 0$ is always larger than for $m = 1$. As for the case of state-to-state integral cross section, this is again an indication that the reaction is favored in nearly collinear collisions. The DCS for $|m| = 1$ is more isotropic than for $m = 0$. For $m = 0$, the DCS is either forward (for $v' = 0$ and 2) or backward scattered (for $v' = 1$), but always with important contributions at intermediate angles.

For $j = 2$ and $|m| = 2$ (corresponding to a narrower initial distribution around 90° than $j = 1$,$m = 1$), the DCS is again rather flat and corresponds to side collisions. In general, the DCS for $m = 0$ is dominant and is the one which varies the most, but the DCS for $m = 1$ is also rather significant and presents an angular dependence similar to that of $m = 0$. The reason is that for $m = 1$, the initial angular dependence is distributed around intermediate configurations between linear and T-shaped.

For $j = 3$, $|m| = 0$ and 1 are always higher than $|m| = 2$ and 3. As m increases, the initial angular distribution presents a lower probability around collinear geometry because spherical harmonics behave as $\sin^m \gamma$ when $\gamma \to 0$ or π. Thus, as m increases, the initial angular distribution is more peaked around $\pi/2$ and the reaction probability decreases. Since the TS is located at $\gamma \approx 70°$, this indicates that the reaction mechanism is more complex, as discussed before.[23] For HF($v = 0$) there must be first an excitation of the HF stretch, favored by nearly collinear collisions, consistent in this case with low m values. Once this is accomplished, the system can bend to reach the TS geometry.

The final angular distribution of the DCS on the different v' is determined by the fast dynamics on the product channel, as a consequence of the DIPR mechanism described above: the transition state is bent, and when the products fly apart, the H atom kicks LiF making it rotate fast. The fast and light H atom may be expelled in any direction, yielding rather broad DCSs. This fast dynamics is however affected by the resonances appearing at low energies which introduces structures in the DCS, specific for each energy and difficult to rationalize. Moreover, the increase of vibrational energy of LiF(v') products slow down significantly the separation between products, thus allowing some rotations, producing more isotropic angular DCS or favoring the backward peaks. In the DIPR mechanism described above, the fast dissociation of H atom is due to the repulsive potential

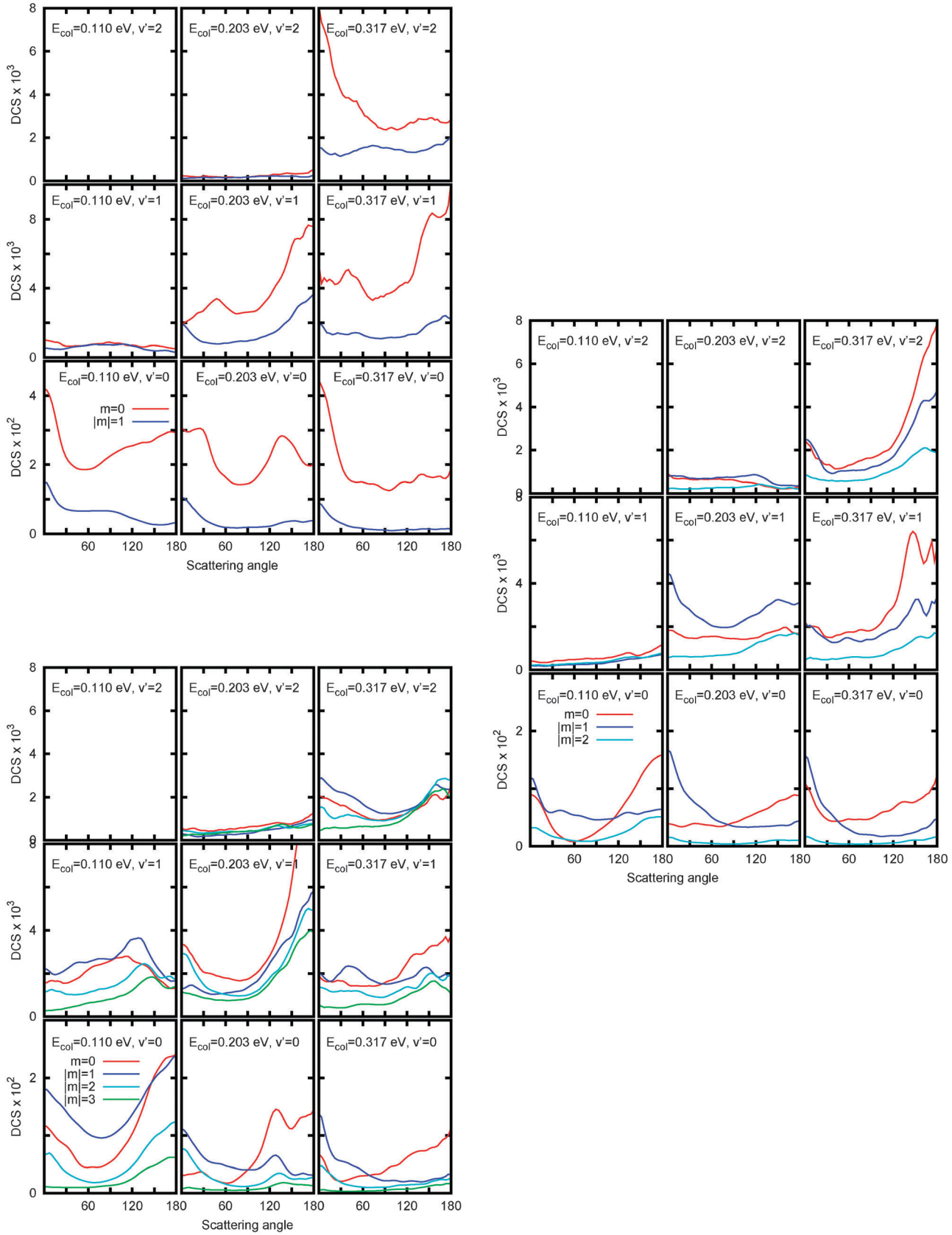

Fig. 7 Vibrationally resolved differential cross section for $j = 1$ (a), 2 (b) and 3 (c), for initial helicities $m = 0,\ldots,j$ and different energies. The results for $m = -|m|$ are identical to those obtained for $m = +|m|$.

of the HF^- subunit within the HF^-Li^+ configuration at the saddle point. This repulsive potential induces a fast separation between H and F^-Li^+. Because of the bent geometry of the saddle point most of rotational excitation can be transferred to the LiF products. This energy exchange is considerably larger than expected from the mass mismatch H/LiF. This may explain why backward scattering may be produced even at the higher energy considered here.

D. Rotational distribution and polarization of products

The LiF products are formed in rather excited rotational state. In Fig. 8 the rotationally resolved DCS are shown for $E = 0.317$ eV and $j = 2$, for several initial m and final v' values. In all cases the rotational distributions are peaked between $j' = 20$ and 30, independently of the final vibrational state v'. It seems that for $v' = 1$, the backward rotational peak is at $j' = 30$ while for $v' = 0$ is at $j' = 20$. The maximum available rotational channels at $E = 0.317$ eV are 50, 42 and 33 for $v' = 0$, 1 and 2, respectively. Clearly, there is no relationship between the available kinetic energy and the final rotational maximum of the distributions. This is explained by the impulsive model used before, in which LiF pushed by the H depart at the saddle point, making it rotate. A similar situation is found for other initial j values[50] and energies.

The analysis of each m' (in reactants frame) or Ω' (in products frame) components is a tedious task. This analysis can be greatly simplified by using a new method of parameterization of the reaction product angular momentum polarization.[24,49,51,75] In this paper we restrict our discussion to the analysis of the rotational orientation and alignment parameters as defined in the theoretical section in eqn (11). These parameters describe the component of the product angular momentum orientation and alignment, with $Q = 0$, parallel to the direction $\mathbf{k}'$ (in products frame) or $\mathbf{k}$ (in reactants frame), and are presented in Fig. 9 and 10 for initial $j = 2$ and $E = 0.317$ eV. These two quantities are obtained using eqn (11), with the scattering amplitudes expressed either in products or reactants frame, respectively. The scattering amplitudes in these two frames are directly related by a simple rotation in the the $\mathbf{k}$–$\mathbf{k}'$ plane (the xz body-fixed plane chosen) given by eqn (3). Therefore, the two

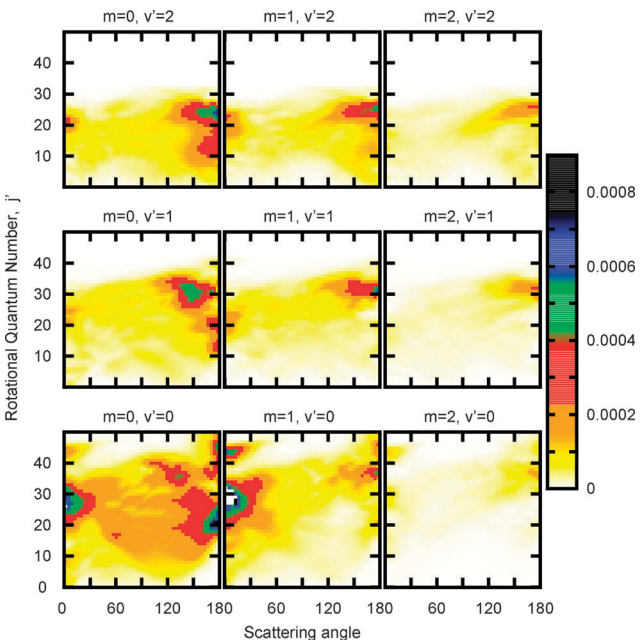

Fig. 8 Rotationally resolved differential cross section for $E = 0.317$ eV, $v = 0$, $j = 2$, and different values of the initial helicity m and final state of products, v'.

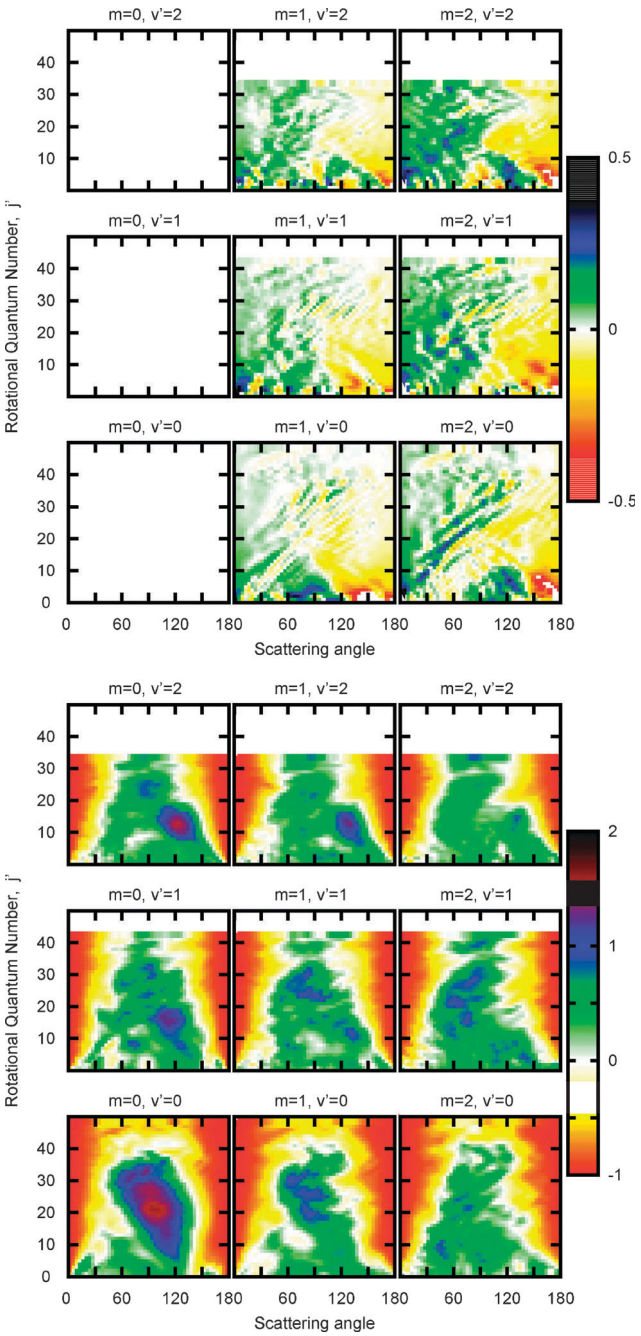

Fig. 9 Orientation (a) and alignment (b) in products frame (with z parallel to $\mathbf{k}'$) as a function of scattering angle and final rotational states, j', for $j = 2$ and $E = 0.317$ eV. Rotationally resolved differential cross section of the initial helicity m and final state of products, v'.

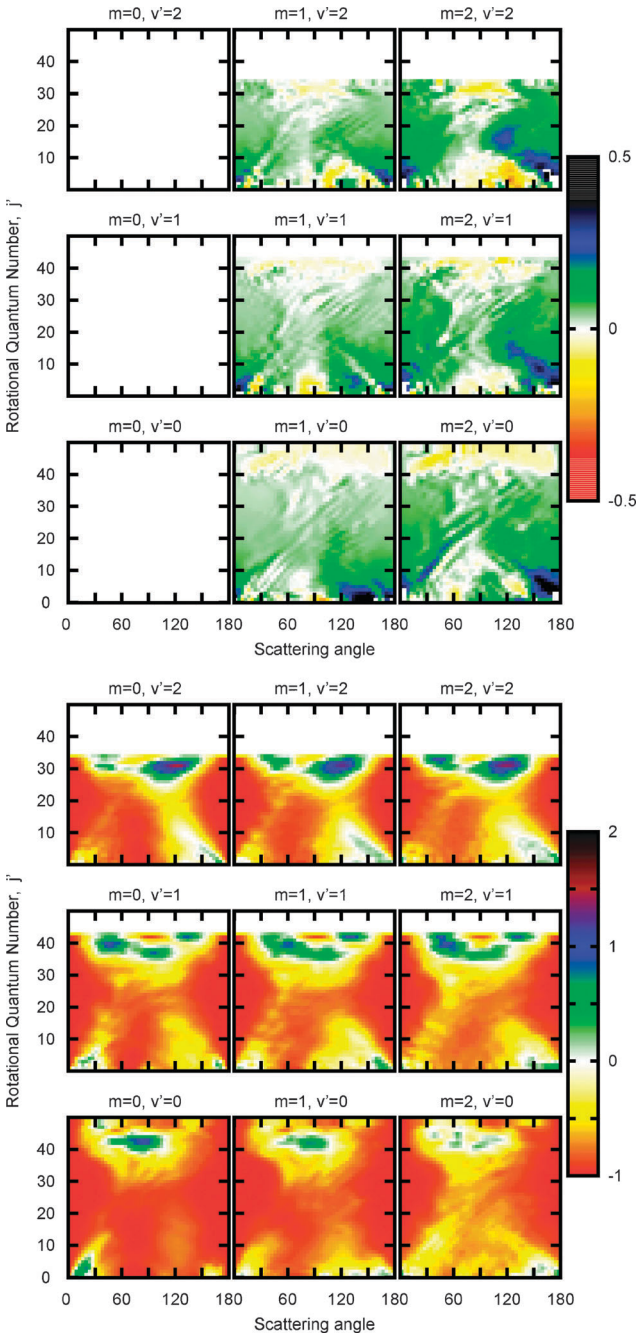

Fig. 10 Same as Fig. 9 but in reactants frame, with z-axis being parallel to **k**, the incoming velocity between reactants.

quantities are related by a geometrical factor. However, since it is not evident to predict the effect on $\mathcal{O}^{j'}_{Q=0}$ and $\mathcal{A}^{j'}_{Q=0}$, they are both shown here to clarify the discussion.

For $m = 0$, the initial HF rotational state has no orientation, and products do not show any angular momentum orientation either, as shown by symmetry and conservation laws.[24,76] A similar situation holds from any initial isotropic distribution of the reactant angular momenta. The orientation obtained for $m > 0$ is non zero as expected, since initial **j** is already oriented along the z-axis, and the depolarizing Coriolis interaction in this case is not effective, as discussed before. For $m < 0$ the product orientation is also non zero, but has opposite sign, so that in case of the reactant initial alignment (*i.e.* $\pm m$ have the same initial population) the net product orientation will become zero after summation. Similarly, in photodissociation the component of the product angular momentum orientation onto the recoil direction can be produced only by using circularly polarized light.[54,77,78]

In the reactant frame, Fig. 10, the sign of the orientation does not vary appreciably with θ. The sign of the orientation $\mathcal{O}^{j'}_{Q=0}$ is preserved with respect to the initial reactant axis **k**. This clearly indicates that **j′** is pointing in the same direction for all scattering angles tending to keep an orientation close to that of the initial **j** vector. This result is also very similar to the case of photodissociation with circularly polarized light where the initial light orientation vector is known to be partly preserved during the reaction and transferred to the angular momentum orientation of the reaction products.[54,79]

On the contrary, in the products frame, Fig. 9, $\mathcal{O}^{j'}_{Q=0}$ corresponds to the projection of the orientation along the z'-axis: it changes sign when the scattering angle θ varies by around $\pi/2$. The reason for this change of sign is merely geometric: **k′** varies with the scattering angle, being parallel/anti-parallel to **k** when the scattering angle is 0/180°. The change of the products reference frame makes the projections of **j′** change too. Thus, if the z'-axis changes direction when varying the scattering angle from 0 to 180°, the projection **Ω′** will change sign. This explains why orientation changes sign in products reference frame.

An interesting thing is that in the semi-classical $j' \gg$ limit, $\langle m' \rangle = \mathcal{O}|j'|$. Here, $\mathcal{O}_{Q'=0} \approx 0.2$ or more for $j' \approx 15$–20, in some cases, so that the corresponding $\langle m' \rangle$ value is 3 or 4. Also, in the backward direction for $0 < j' < 10$ the orientation reaches a value of 0.5, consistent with $m' \approx 5$ for $j' = 10$. The orientation initially set for reactants is slightly reduced for products. However, the average helicity changes from $m = 2$ to $m' = 4$ or 5, an effect that can only be attributed to the reaction dynamics. A similar situation was found in the photodissociation of ICN,[77,80] in which final CN fragments, with rotational angular momentum of $\approx$40, were measured to have an average projection of 7, while the initial helicity introduced by the photon is only of 1 quantum.

The alignment of products rotational states with respect to **k**, in Fig. 10, is independent of the initial m, and nearly always close to -1, indicating that **j′** is perpendicular to **k**. This is easily understood using a simple kinematic model based on the angular momentum conservation from reactants to products, *i.e.* $\mathbf{j} + \ell = \mathbf{j}' + \ell'$. **j** is in general rather small and can be neglected, *i.e.* $\ell \approx \mathbf{j}' + \ell'$. Since ℓ and ℓ' are perpendicular to **k** and **k′**, respectively, they are both perpendicular to the scattering plane. Therefore, **j′** is also expected to be perpendicular to that plane. This is also consistent with the DIPR mechanism, in which LiF is produced in highly excited rotational states by the strong repulsive state of the HF^- subunit within the HF^-Li^+ bent transition state. This mechanism is based on the topology of the potential energy surface and is due to the reaction dynamics, and can be rather general in A + BC reactions. These results are in agreement with recent QCT calculations performed for this system.[81]

When the alignment is expressed in the products frame, along the $\mathbf{k}'$ axis, it is no longer constant but it varies with the scattering angle, as previously reported for $j = 0$.[50] For forward and backward scattering, the alignment is negative, close to -1, indicating that low Ω' values are preferred, meaning that $\mathbf{j}'$ tends to be perpendicular to $\mathbf{k}'$. On the contrary, for side angles, the alignment is close to 2, indicating that the preferred axis of rotation changes now to be parallel to $\mathbf{k}'$. This behavior is also explained by the change of the direction of the z'-axis when moving from 0 to 90° scattering angles, and is due to geometric effects. This also indicates that the reactants frame, with the z-axis parallel to $\mathbf{k}$ express more naturally the main vector properties of the products polarization.

The final alignment of $\mathbf{j}'$ is independent of the initial projection m, the projection of the reactant angular momentum $\mathbf{j}$, and therefore m can be neglected. However, the initial value of m determines the orientation of products, as discussed above. At scattering angles of 0 and π, where $\mathbf{k}$ and $\mathbf{k}'$ are parallel or anti-parallel, the initial helicity m can only be transferred to $\mathbf{j}'$, since ℓ' is perpendicular by definition to $\mathbf{k}'$. At other scattering angles this condition is not fulfilled, but this propensity seems to hold.

The general trends of the product polarization discussed so far are essentially valid for other energies. This indicates that the kinematic arguments used above are rather strict on average and explains the limiting values obtained for the orientation and alignment. It should be noted, however, that the values obtained are not strictly the limiting values, and there is some dependence on the scattering angle and on the energy. These deviations, more evident for lower j values, are the traces of the reaction dynamics, not explained by the simple kinematic models used above. It is therefore important to analyse them in more detail to get a further insight of the reaction dynamics.

IV. Conclusions

In this work the first quantum simulation of the state-to-state differential cross section of the Li + HF($v = 0$,$j = 0$,1,2,3m) → LiF(v',j',Ω') + H reaction is performed, using exact wave packet methods and the most accurate PES currently available.[68] The obtaining of differential cross sections as a function of the initial relative orientation of reactants and determining the polarization of products provides a clear picture of the reactive collision process, which can be nicely explained by the properties of the transition state.

The total integral cross section for several rotational states has been calculated and compared with experimental results of Loesch and co-workers.[20,21] The differential cross section in the center-of-mass have been presented for different initial states, including different initial helicities of the entrance channel. For $m = 0$ the cross section is significantly larger than for $m = j$, showing that the reaction is favored by head-on collisions.

The differential cross section shows a preference for forward and backward scattering, but the side-scattering is also significant. The DCS obtained for lower energies present specific structures associated with either tunneling or TS resonances. This makes it difficult to rationalize them in terms of simple models. For this reason we focused on the highest energy considered, 0.317 eV, at which resonances play a minor role. For this energy, the scattering is forward for $v' = 0$, while it becomes backward for $v' = 1$ and 2. This can be explained by an impulsive model in which H dissociates fast from the bent Li^+F^-H transition state. The internuclear interaction within the HF^- is repulsive, making possible a relatively large energy transfer between the light H atom and the heavy LiF molecule. Thus, when H leaves in the forward direction, it pushes F backward, introducing a force against the direction of LiF motion which is the origin of the vibrational excitation. On the contrary, when H leaves in the backward direction, it pushes forward LiF, *i.e.* in the same direction of its motion, without producing vibrational excitation.

The bent geometry of the transition state explains the high rotational excitation of LiF products obtained for all final vibrational states v', independently of the available kinetic energy.

This impulsive model also explains the polarization of the rotational states of products: the alignment is nearly constant with the scattering angle and equal to -1 (in reactants frame), indicating that $\mathbf{j}'$ is perpendicular to $\mathbf{k}$, as also found recently using QCT for this reaction.[81] When an orientation is created in the HF reactants, by setting for example a single $m \neq 0$, the LiF products also present an orientation in the same direction or rotation, which is even amplified by the reaction dynamics for high j' values.

This simple picture of the polarization of $\mathbf{j}'$ when expressed in the reactants frame gets far more complicated when transforming to products frame. The reason is that the z'-axis in products frame changes with the scattering angle, inverting its direction when passing from 0 to 180°. These results may be, however, not completely general to A + BC reactions and should be analyzed in detail.

The analysis of the dynamics at lower energies deserves further attention because the simple model used here becomes complicated by the resonances, tunneling or TS that appear there.

The study of the quantum stereo-dynamics offers not only a way to unravel the complex dynamics involved in a reaction but also a way to control its outcome. For example, the possibility of orienting reactants can produce an enhancement of the reactivity as discussed in this work and detected experimentally.[11,12,14] In this case, the hyperfine coupling produces a depolarization which should be taken into account in future simulations. Experimentally the hyperfine coupling is switched off by adding weak electric fields along the center-of-mass vector.[14] Another source of control is the use of coherent superposition of different helicity states, properly designed for this purpose.

Acknowledgements

We want to acknowledge Drs Susana Gómez-Carrasco and Jesús Aldegunde for their help and very fruitful discussions. This work has been supported by the Ministerio de Ciencia e Innovación, under grants CSD2009-00038 (programa CONSOLIDER-INGENIO 2010 entitled "Molecular Astrophysics: the Herschel and Alma era"), FIS2010-18132,

CTQ2008-02578 and CTQ2007-62898, and by Comunidad Autónoma de Madrid (CAM) under Grant No. S-0505/MAT/0303. The calculations have been performed in CESGA computers, and we also acknowledge for a grant for computer time there.

References

1 D. R. Case and D. R. Herschbach, *Mol. Phys.*, 1975, **30**, 1537.
2 G. M. McClelland and D. R. Herschbach, *J. Phys. Chem.*, 1979, **83**, 1445.
3 P. Casavecchia, N. Balucani and G. G. Volpi, *Annu. Rev. Phys. Chem.*, 1999, **50**, 347.
4 K. Liu, *Annu. Rev. Phys. Chem.*, 2001, **52**, 139.
5 X. Yang, *Int. Rev. Phys. Chem.*, 2005, **24**, 37.
6 D. S. Y. Hsu, N. D. Weinstein and D. R. Herschbach, *Mol. Phys.*, 1975, **29**, 257.
7 M. Brouard, H. M. Lambert, S. P. Rayner and J. P. Simons, *Mol. Phys.*, 1996, **89**, 403.
8 J. Aldegunde, M. P. de Miranda, J. M. Haigh, B. K. Kendrick, V. Sáez-Rabanos and F. J. Aoiz, *J. Phys. Chem. A*, 2005, **109**, 6200.
9 S. Stolte, *Ber. Bunsenges. Phys. Chem.*, 1982, **86**, 413.
10 D. H. Parker and R. B. Bernstein, *Annu. Rev. Phys. Chem.*, 1989, **40**, 561.
11 R. N. Zare, *Ber. Bunsenges. Phys. Chem.*, 1982, **86**, 422.
12 H. J. Loesch and F. Stienkemeier, *J. Chem. Phys.*, 1993, **98**, 9570.
13 B. Friedrich and D. R. Herschbach, *Z. Phys.*, 1991, **18**, 153.
14 H. J. Loesch, *Annu. Rev. Phys. Chem.*, 1995, **46**, 555.
15 D. R. Herschbach, *Adv. Chem. Phys.*, 1966, **10**, 319.
16 H. J. Loesch, E. Stenzel and B. Wüstenbecker, *J. Chem. Phys.*, 1991, **95**, 3841.
17 H. J. Loesch and F. Stienkemeier, *J. Chem. Phys.*, 1993, **99**, 9598.
18 F. J. Aoiz, E. Verdasco, V. Sáez-Rábanos, H. J. Loesch, M. Menéndez and F. Stienkemeier, *Phys. Chem. Chem. Phys.*, 2000, **2**, 541.
19 C. H. Becker, P. Casavecchia, P. W. Tiedemann, J. J. Valentini and Y. T. Lee, *J. Chem. Phys.*, 1980, **73**, 2833.
20 O. Höbel, M. Menéndez and H. J. Loesch, *Phys. Chem. Chem. Phys.*, 2001, **3**, 3633.
21 O. Hobel, R. Bobbenkamp, A. Paladini, A. Russo and H. J. Loesch, *Phys. Chem. Chem. Phys.*, 2004, **6**, 2198.
22 R. Bobbenkamp, A. Paladini, A. Russo, H. J. Loesch, M. Menéndez, F. J. Aoiz E. Verdasco and H. J. Werner, *J. Chem. Phys.*, 2005, **122**, 244304.
23 M. Lara, A. Aguado, O. Roncero and M. Paniagua, *J. Chem. Phys.*, 1998, **109**, 9391.
24 M. P. de Miranda, F. J. Aoiz, L. Bañares and V. Sáez-Rábanos, *J. Chem. Phys.*, 1999, **111**, 5368.
25 F. J. Aoiz, M. T. Martínez and V. Sáez-Rábanos, *J. Chem. Phys.*, 2001, **114**, 8880.
26 J. M. Alvariño, V. Aquilanti, S. Cavalli, S. Crocchianti, A. Laganà and T. Martínez, *J. Chem. Phys.*, 1997, **107**, 3339.
27 J. M. Alvariño, V. Aquilanti, S. Cavalli, S. Crocchianti, A. Laganà and T. Martínez, *J. Phys. Chem. A*, 1998, **102**, 9638.
28 D. Skouteris, S. Crocchianti and A. Laganà, *Chem. Phys. Lett.*, 2007, **440**, 1.
29 D. Skouteris, S. Crocchianti and A. Laganà, *Chem. Phys.*, 2008, **349**, 170.
30 A. Aguado, C. Suárez and M. Paniagua, *Chem. Phys.*, 1995, **201**, 107.
31 G. A. Parker, A. Laganà, S. Crocchianti and R. T Pack, *J. Chem. Phys.*, 1995, **102**, 1238.
32 A. Aguado, M. Paniagua, M. Lara and O. Roncero, *J. Chem. Phys.*, 1997, **107**, 10085.
33 R. Burcl, P. Piecuch, V. Spirko and O. Bludský, *Int. J. Quantum Chem.*, 2000, **80**, 916.
34 A. W. Jasper, M. D. Hack, D. G. Truhlar and P. Piecuch, *J. Chem. Phys.*, 2002, **116**, 8353.
35 A. Aguado, M. Paniagua, C. Sanz-Sanz and O. Roncero, *J. Chem. Phys.*, 2003, **119**, 10088.
36 J. M. Alvariño, P. Casavecchia, O. Gervasi and A. Laganà, *J. Chem. Phys.*, 1982, **77**, 6341.
37 F. J. Aoiz, M. T. Martínez, M. Menéndez, V. Sáez-Rábanos and E. Verdasco, *Chem. Phys. Lett.*, 1999, **299**, 25.
38 D. L. Miller and R. E. Wyatt, *J. Chem. Phys.*, 1987, **86**, 5557.
39 M. Baer, E. García, A. Laganà and O. Gervasi, *Chem. Phys. Lett.*, 1989, **158**, 362.
40 M. Baer, I. Last and H. J. Loesch, *J. Chem. Phys.*, 1994, **101**, 9648.
41 A. Laganà, A. Bolloni and S. Crocchianti, *Phys. Chem. Chem. Phys.*, 2000, **2**, 535.
42 F. Gogtas, G. G. Balint-Kurti and A. R. Offer, *J. Chem. Phys.*, 1996, **104**, 7927.
43 A. Aguado, M. Paniagua, M. Lara and O. Roncero, *J. Chem. Phys.*, 1997, **106**, 1013.
44 W. Zhu, D. Wang and J. Z. H. Zhang, *Theor. Chem. Acc.*, 1997, **96**, 31.
45 M. Lara, A. Aguado, M. Paniagua and O. Roncero, *J. Chem. Phys.*, 2000, **113**, 1781.
46 D. Q. Xie, S. M. Li and H. Guo, *J. Chem. Phys.*, 2002, **116**, 6391.
47 P. F. Weck and N. Balakrishnan, *J. Chem. Phys.*, 2005, **122**, 154309.
48 P. F. Weck and N. Balakrishnan, *J. Chem. Phys.*, 2005, **122**, 234310.
49 M. P. de Miranda and D. C. Clary, *J. Chem. Phys.*, 1997, **106**, 4509.
50 A. Zanchet, O. Roncero, T. González-Lezana, A. Rodríguez-López, A. Aguado, C. Sanz-Sanz and S. Gómez-Carrasco, *J. Phys. Chem. A*, 2009, **113**, 14488.
51 G. G. Balint-Kurti and O. Vasyutinjskii, *J. Phys. Chem. A*, 2009, **113**, 14281.
52 M. H. Alexander and S. L. Davis, *J. Chem. Phys.*, 1983, **79**, 227.
53 K. Blum, *Density matrix theory and applications*, Plenum, New York, 2nd edn, 1996.
54 L. D. A. Siebbeles, M. Glass-Maujean, O. S. Vasyutinskii, J. A. Beswick and O. Roncero, *J. Chem. Phys.*, 1994, **100**, 3610.
55 U. Fano, *Rev. Mod. Phys.*, 1957, **29**, 74.
56 R. N. Zare, *Angular Momentum*, John Wiley and Sons, Inc., 1988.
57 G. C. Schatz and A. Kuppermann, *J. Chem. Phys.*, 1976, **65**, 4642.
58 J. Z. H. Zhang and W. H. Miller, *J. Chem. Phys.*, 1989, **91**, 1528.
59 M. S. Child, *Molecular Collision Theory*, Dover Publications, Inc., 1996.
60 Y. Huang, D. J. Kouri and D. K. Hoffman, *J. Chem. Phys.*, 1994, **101**, 10493.
61 V. A. Mandelshtam and H. S. Taylor, *J. Chem. Phys.*, 1995, **103**, 2903.
62 Y. Huang, S. S. Iyengar, D. J. Kouri and D. K. Hoffman, *J. Chem. Phys.*, 1996, **105**, 927.
63 G. J. Kroes and D. Neuhauser, *J. Chem. Phys.*, 1996, **105**, 8690.
64 R. Chen and H. Guo, *J. Chem. Phys.*, 1996, **105**, 3569.
65 S. K. Gray and G. G. Balint-Kurti, *J. Chem. Phys.*, 1998, **108**, 950.
66 S. Gómez-Carrasco and O. Roncero, *J. Chem. Phys.*, 2006, **125**, 054102.
67 T. González-Lezana, A. Aguado, M. Paniagua and O. Roncero, *J. Chem. Phys.*, 2005, **123**, 194309.
68 A. Aguado, M. Paniagua and H. J. Werner, Unpublished, http://www.theochem.uni-stuttgart.de/werner/lihf/lihf.html, 2004.
69 J. C. Polanyi and W. H. Wong, *J. Chem. Phys.*, 1969, **51**, 1439.
70 M. H. Mok and J. C. Polanyi, *J. Chem. Phys.*, 1969, **51**, 1451.
71 A. Laganà, M. L. Hernández and J. M. Alvariño, *Chem. Phys. Lett.*, 1984, **106**, 41.
72 J.-M. Mestdagh, B. Soep, M.-A. Gaveu and J.-P. Visitcot, *Int. Rev. Phys. Chem.*, 2003, **22**, 285.
73 R. D. Levine and R. B. Bernstein, *Molecular Reaction Dynamics and Chemical Reactivity*, Oxford University Press, 1987.
74 M. Paniagua, A. Aguado, M. Lara and O. Roncero, *J. Chem. Phys.*, 1998, **109**, 2971.
75 M. P. de Miranda, D. C. Clary, J. F. Castillo and D. E. Manolopoulos, *J. Chem. Phys.*, 1998, **108**, 3142.
76 J. Aldegunde, PhD thesis, *Stereodynamics of elementary reactions: effect of the reagent's rotational angular momentum polarization*, 2007.
77 J. A. Beswick, M. Glass-Maujean and O. Roncero, *J. Chem. Phys.*, 1992, **96**, 7514.
78 A. G. Suits and O. S. Vasyutinskii, *Chem. Rev.*, 2008, **108**, 3706.
79 O. S. Vasyutinskii, *Sov. Phys. JETP*, 1981, **54**, 855.
80 E. Hasselbrink, J. R. Waldeck and R. N. Zare, *Chem. Phys.*, 1988, **126**, 191.
81 M.-H. Yuan and G.-J. Zhao, *Int. J. Quantum Chem.*, 2010, **110**, 1842.